A paper for the special issue of JETP devoted to the centenary of A.E. Chudakov

Cosmic-Ray Research at the TAIGA Astrophysical Facility: Results and Plans

**I. I. Astapov[d], P. A. Bezyazeekov[b], M. Blank[m], E. A. Bonvech[a], A. N. Borodin[c], M. Brückner[l],
N. M. Budnev[b], A. V. Bulan[a], A. Vaidyanathan[e], R. Vishnevsky[l], N. V. Volkov[i], P. A. Volchugov[a],
D. M. Voronin[f], A. R. Gafarov[b], O. A. Gress[b], T. I. Gress[b], O. G. Grishin[b], A. Yu. Garmash[e,h],
V. M. Grebenyuk[c,j], A. A. Grinyuk[c], A. N. Dyachok[b], D. P. Zhurov[b], A. V. Zagorodnikov[b],
A. L. Ivanova[b,h], N. N. Kalmykov[a], V. V. Kindin[d], S. N. Kiryukhin[b], R. P. Kokoulin[d], K. G. Kompaniets[d],
E. E. Korosteleva[a], V. A. Kozhin[a], E. A. Kravchenko[e,h], A. P. Kryukov[a], L. A. Kuzmichev[a,*],
A. Chiavassa[n], A. A. Lagutin[i], M. V. Lavrova[c], Yu. E. Lemeshev[b], B. K. Lubsandorzhiev[f],
N. B. Lubsandorzhiev[a], R. R. Mirgazov[b], R. Mirzoyan[k], R. D. Monkhoev[b], E. A. Osipova[a],
A. L. Pakhorukov[b], A. Pan[c], M. I. Panasyuk[a†], L. V. Pankov[b], A. A. Petrukhin[d], D. A. Podgrudkov[a],
V. A. Poleshchuk[b], E. G. Popova[a], A. Porelli[l], E. B. Postnikov[a], V. V. Prosin[a], V. S. Ptuskin[g],
A. A. Pushnin[b], A. V. Razumov[a], R. I. Raikin[i], G. I. Rubtsov[f], E. V. Ryabov[b], Ya. I. Sagan[c,j],
V. S. Samoliga[b], I. Satyshev[c], A. A. Silaev[a], A. A. Silaev (Jr.)[a], A. Yu. Sidorenkov[f], A. V. Skurikhin[a],
A. V. Sokolov[e,h], L. G. Sveshnikova[a], Ya. V. Suvorkin[b], V. A. Tabolenko[b], A. B. Tanaev[b],
B. A. Tarashchansky[b], M. Yu. Ternovoi[b], L. G. Tkachev[c,j], M. Tluczykont[m], N. A. Ushakov[f],
D. Horns[m], D. V. Chernov[a], and I. I. Yashin[d]**

[a]*Skobeltsyn Institute of Nuclear Physics, Moscow State University, Moscow, 119991 Russia*
[b]*Institute of Applied Physics, Irkutsk State University, Irkutsk, 664003 Russia*
[c]*Joint Institute for Nuclear Research, Dubna, Moscow obl., 141980 Russia*
[d]*National Research Nuclear University MePhi, Moscow, 115409 Russia*
[e]*Novosibirsk State University, Novosibirsk, 630090 Russia*
[f]*Institute for Nuclear Research, Russian Academy of Sciences, Moscow, 117312 Russia*
[g]*Pushkov Institute of Terrestrial Magnetism, Ionosphere, and Radio Wave Propagation,
Russian Academy of Sciences, Moscow, 108840 Russia*
[h]*Institute of Nuclear Physics, Russian Academy of Sciences, Siberian Branch, Novosibirsk, 630090 Russia*
[i]*Altai State University, Barnaul, 656049 Russia*
[j]*Dubna University, Dubna, Moscow obl., 141982 Russia*
[k]*Max Planck Institute for Physics, München, 80804 Germany*
[l]*DESY, Zeuthen, 15738 Germany*
[m]*Hamburg University, Hamburg, 20148 Germany*
[n]*University of Turin, Turin, 10124 Italy*
**e-mail: kuz@dec1.sinp.msu.ru*

Abstract—High-energy cosmic-ray research via the detection of Cherenkov radiation from extensive air showers was begun in the Tunka valley (50 km to the west from the southern extremity of Lake Baikal) in the early 1990s. A series of large arrays combined into the TAIGA (Tunka Advanced Instrument for cosmic-ray physics and Gamma Astronomy) astrophysical facility and designed to study gamma rays and charged cosmic rays have been created in the elapsed time. Descriptions of the facility arrays and the main results obtained while investigating high-energy cosmic rays are presented. Plans for a further development of the astrophysical facility are discussed.
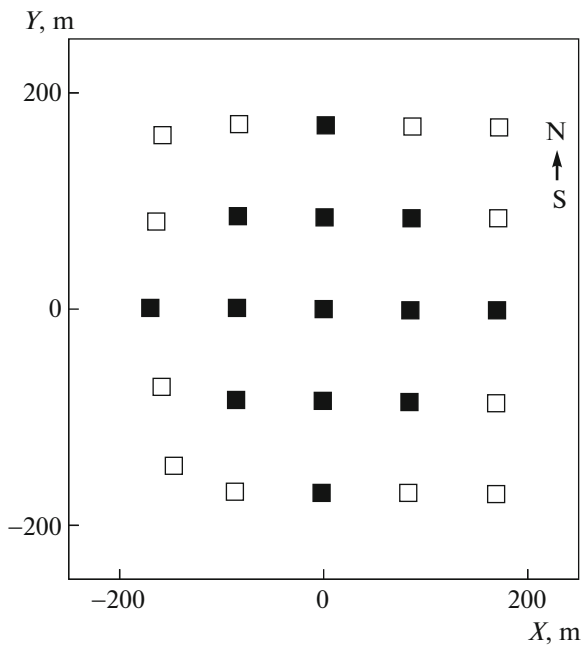
1. INTRODUCTION

Progress in understanding the nature of high and ultra-high-energy cosmic-ray sources located in both

---

† Deceased.

our Galaxy and the Metagalaxy follows three directions:

(1) the study of secondary gamma-ray photons produced by cosmic rays (CRs) in the immediate neighborhood of the source where CRs are accelerated;

Fig. 1. The arrangement of detectors in the Tunka-25 array. The black squares indicate the detectors involved in triggering the array.

(2) the detection of high-energy neutrinos produced during the interactions of high-energy particles in sources;

(3) an accurate determination of the CR energy spectrum, mass composition, and anisotropy through the detection of extensive air showers (EASs).

The TAIGA astrophysical facility [1, 2] allows the nature of CR sources to be investigated within both the first and the third approaches. A unique feature of the facility consists in combining arrays with detectors of different types into a unified system to detect all EAS components. This will allow one to search for PeVatrons, i.e., galactic objects in which protons are accelerated to energies $\sim 10^{15}-10^{17}$ eV, to find the energy limits for particle acceleration in supernova remnants and pulsar nebulae, and to carry out a search for correlations with neutrino events recorded by the Ice-Cube [3] and Baikal-GVD [4] neutrino observatories. In this paper we will discuss only the results obtained within the third of the listed approaches when measuring the energy spectrum and mass composition through the detection of EASs.

Studying the energy spectrum and mass composition of primary CRs in the energy range $10^{14}-10^{18}$ eV is of crucial importance for understanding the origin and propagation of CRs in the Galaxy. The increasing predominance of heavy nuclei from the "knee" energy to 10^{17} eV points to the energy limit for CR acceleration in the standard model of particle acceleration in supernova remnants (for a review, see [5]). At higher energies the

mass composition again becomes lighter at 2×10^{18} eV. This may point to the transition to an extragalactic origin of CRs or the dominance of new galactic sources of an unknown nature (for a discussion, see [6, 7]).

The paper has the following structure. The main arrays of the astrophysical facility, including the arrays that are already nonoperational at present, are briefly described in Section 2. The EAS parameter reconstruction methods are presented in Section 3. Our main results are presented in Section 4.

2. DEVELOPMENT OF THE ASTROPHYSICAL FACILITY IN THE TUNKA VALLEY

2.1. The First Experiments (1993–2005)

The experiments to detect EASs by their Cherenkov radiation in the Tunka valley 50 km to the west from Lake Baikal (51.49 N, 103.04 E) were begun in 1993. The first experimental array Tunka-4 consisted of four optical detectors [8]. Hybrid QUASAR-370 photomultiplier tubes (PMTs) with a photocathode diameter of 37 cm designed for the Baikal neutrino telescope NT200 [9] were used in the optical detectors of the array.

The next array Tunka-13 consisted of 13 detectors based on PMTs of the same type and operated from 1996 to 1999. In 2000 the number of detectors was increased to 25. This array called Tunka-25 [10] operated until 2005. The detectors of the array were located at the grid points of a square grid with a 85-m spacing on an area ~ 0.1 km^2 (Fig. 1).

Below we briefly describe the arrays that have operated and are operating in the astrophysical facility since 2005. At present, the following arrays operate in the facility: Tunka-133, Tunka-Grande, TAIGA-HiS-CORE, TAIGA-MUON, and TAIGA-IACT. All these arrays of the facility are synchronized with one another with a 10-ns precision [11].

2.2. Tunka-133

The Tunka-133 array consists of 175 Cherenkov detectors [12, 13] arranged over an area of 3 km^2 (Fig. 2). The detectors are grouped into 25 clusters of seven detectors each — six detectors at the vertices of a regular hexagon and one at the center. The detector spacing in one cluster is 85 m. Nineteen clusters are arranged in the form of a dense central part of the array with a radius ~ 500 m. These 133 detectors gave the name Tunka-133 to the array. The remaining 6 outer clusters are located at a distance ~ 1 km around the center. Each cluster is an independent array with its own local trigger. Each detector contains a PMT with a photocathode diameter of 20 cm the signal from which is sent to the cluster center, where it is digitized by a 12-bit ADC with a sampling frequency of 200 MHz. The main task of the Tunka-133 array is to
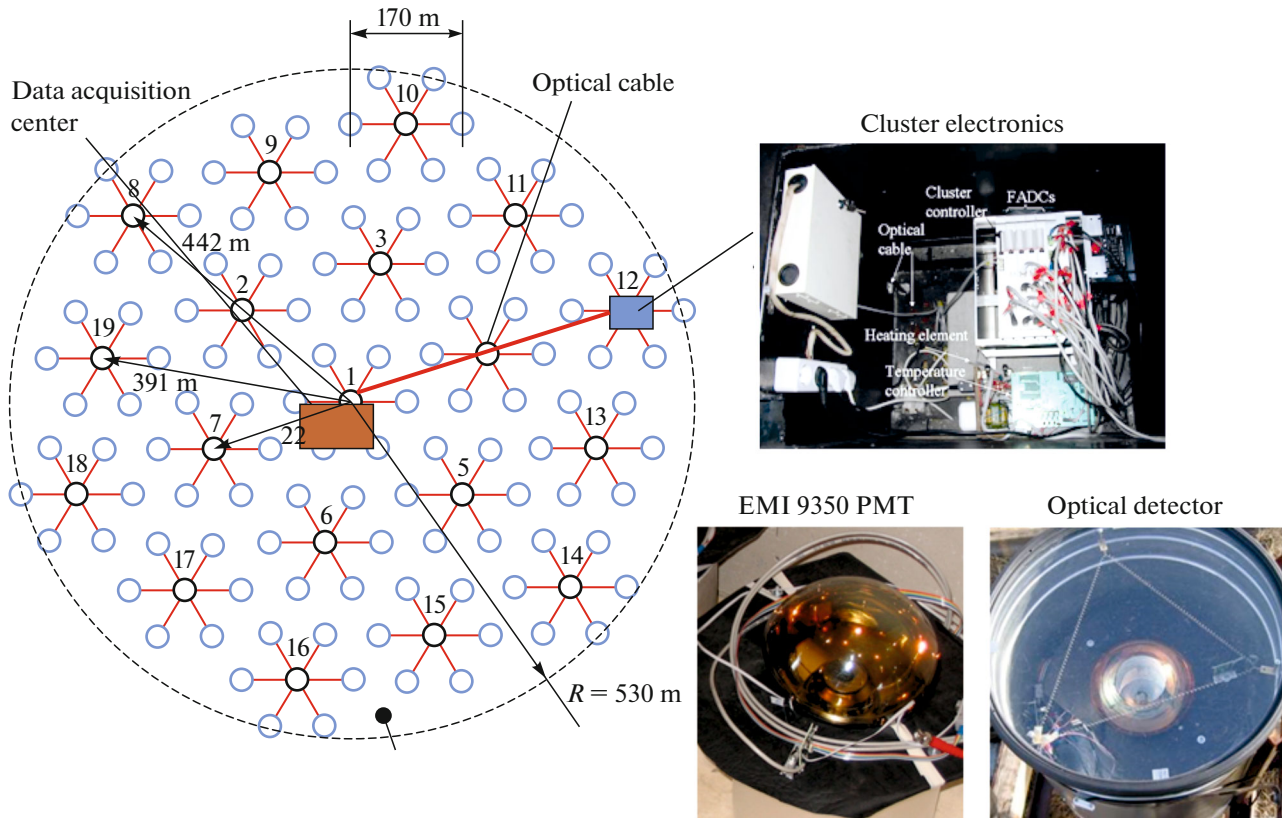
Fig. 2. The arrangement of detectors in the central part of the Tunka-133 array.

investigate the energy spectrum and mass composition of CRs with energies above 10^{16} eV. The EAS parameter reconstruction methods and the main results will be presented in Sections 3 and 4.

2.3. Tunka-Grande

The Tunka-Grande array [14] is a network of scintillation detectors combined into 19 stations, each of which consists of the ground and underground parts. The ground part contains 12 counters with a total area ~8 m² that detects charged EAS particles. The underground part located under a 1.5-m-thick layer of soil consists of 8 counters with a total area ~5 m² and is designed to detect the EAS muon component. The scintillation station electronics, which is analogous to the Tunka-133 electronics, provides local station trigger generation, signal shape digitization with a 5-ns step, and data transmission to the unified data acquisition center.

2.4. TAIGA−HiSCORE

The TAIGA-HiSCORE (High Sensitivity COsmic Rays and gamma Explorer) array [15, 16] is a network of wide-field optical stations to detect the Cherenkov radiation from EASs. At present, the array consists of 120 stations arranged on an area of 1.1 km², with the station spacing being 106 m (Fig. 3). The stations are grouped into 4 clusters with independent data acquisition centers. Each station is connected with the cluster data acquisition center by a fiber-optic cable for data transmission and synchronization [11]. One optical station contains four PMTs with a diameter of 20 cm (ET 9352 and Hamamatsu R5912). The light collection area of each PMT was increased by a factor of 4 using a Winston cone with a diameter of 0.4 m and a viewing angle of 30° (a solid angle of 0.6 sr). The signals from the PMT anode and intermediate dynode are digitized with a 0.5-ns step. The effective energy threshold of the array when four or more stations are triggered is ~80 TeV for EASs from charged CR particles and ~40 TeV for EASs from gamma-ray photons. The angular resolution of the array changes from 0.4−0.5 deg. near the array threshold to 0.1 deg. when more than 10 stations are triggered [17]. The TAIGA-HiSCORE array was created not only to investigate CRs, but also to search for local high-energy gamma-ray sources [18]. The large angular aperture of the array and its good angular resolution have made it possible to begin a search for astrophysical nanosecond optical transients [19].
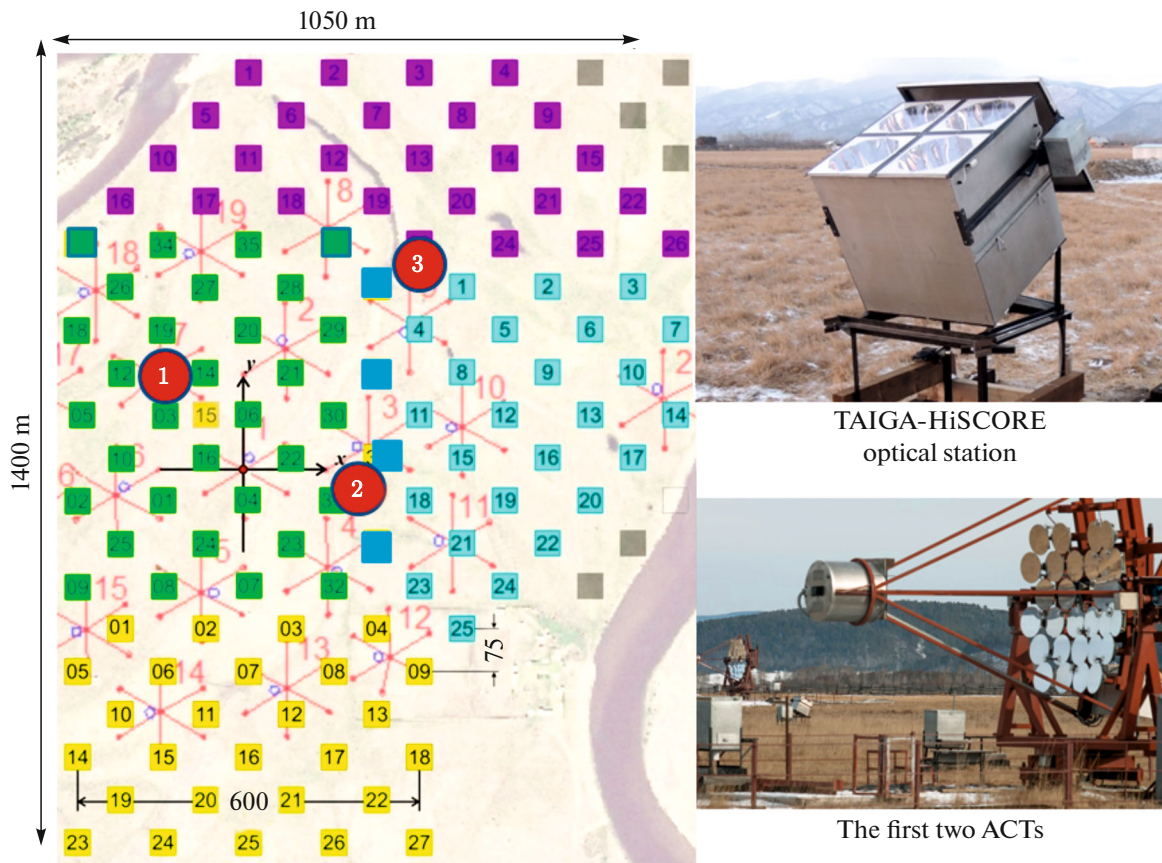
Fig. 3. Left: the arrangement of optical stations of the TAIGA-HiSCORE array (squares) and three ACTs of the TAIGA-IACT array (circles). Right: the TAIGA-HiSCORE optical station and the first two ACTs.

2.5. Tunka-REX

The detection of radio emission is yet another method that can be used to reconstruct the EAS parameters. The radio emission arises mainly from the current produced by the separation of relativistic electrons and positrons of a shower in the geomagnetic field. The Tunka-REX (Radio Extension) array [20] is a system of antennas that operated for 7 years (2012–2019) in the astrophysical facility [21] and was used in experiments to detect the radio emission from EASs. The array consisted of 63 radio antennas arranged on an area of 3 km^2. The antennas were connected to FADC boards in the data acquisition electronics of the Tunka-133 and Tunka-Grande arrays. The signals from the antennas were read out when Tunka-133 and Tunka-Grande local triggers were generated.

2.6. TAIGA−Muon

A new array, TAIGA-Muon [22], is being created to investigate the mass composition of CRs with energies above 10^{16} eV and to suppress the hadron background when detecting high-energy gamma-ray photons. New scintillation counters with an area of 1 m^2

were designed for this array [23]. The design of the counters allows them to be buried in soil without any additional protection. The first three clusters of the TAIGA-Muon array were deployed in 2019. Each cluster has 8 ground and as many underground detectors. The counters are arranged in pairs; the ground ones are located strictly above the underground ones. All 8 pairs are arranged along the perimeter of a square with a 5-m side. The distance between the neighboring pairs is 1 m. The area of the muon detectors in the TAIGA-Muon array is planned to be increased to 150 m^2 by 2024.

2.7. TAIGA−IACT

Five atmospheric Cherenkov telescopes (ACTs) with the reconstruction of the angular distribution (image) of Cherenkov light from EASs are planned to be deployed in the astrophysical facility. Such telescopes are the main instruments of ground-based high-energy gamma-ray astronomy that allow the events from gamma-ray photons to be separated from the events from charged CR particles. The first two telescopes already operate; the third telescope will begin to operate in the winter of 2022. The fourth and

fifth telescopes will begin to operate by 2023. Each ACT of the TAIGA-IACT (Imaging Atmospheric Cherenkov Telescope) array has composite Davis–Cotton mirrors with an area ~10 m^2 and a focal length of 4.75 m [24]. Imaging cameras consisting of 600 PMTs with a photocathode diameter of 2 cm each (XP1911) are installed at the mirror focus. The diameter of the cameras is ~110 cm. The camera viewing angle is 9.6°, the viewing angle per pixel is 0.36°, and the point spread function (PSF) of the telescope is ~0.07° [24]. The imaging camera and the data acquisition system are described in detail in [25]. Our telescopes correspond in their characteristics to the Small Size Telescopes (SSTs) of the CTA project [26]. The viewing angle of such telescopes is more than twice the viewing angle of previous-generation telescopes. Such a viewing angle allows EASs with an axis position up to 500 m from the telescope to be detected. The telescope energy threshold is 2–3 TeV, depending on the zenith angle at which the gamma-ray source is seen. At energies above 10 TeV it becomes possible to use a stereoscopic approach — EASs from gamma-ray photons are detected by two or more telescopes [27]. At energies above 40 TeV a new "hybrid" approach to the detection of gamma-ray photons becomes possible — the detection of EASs both by the telescopes and by the TAIGA-HiSCORE array. The main advantage of the joint operation of the ACTs and the network of wide-field Cherenkov stations is a more efficient selection of events from gamma-ray photons from the EAS background from charged CRs [28].

2.8. Small Cherenkov Telescopes

One of the shortcomings of the joint operation of the TAIGA-HiSCORE array and the Cherenkov telescopes is a significant difference in apertures. The ACT aperture is a factor of 20 smaller than that of the TAIGA-HiSCORE array and, accordingly, only 5% of the events recorded by the TAIGA-HiSCORE array fall into the ACT field of view. Small Cherenkov telescopes with cameras with a field-of-view diameter of 25–30 deg and an effective detection area ~1 m^2 are planned to be used to investigate the range of energies above 50 TeV. During the operation of such telescopes, the percentage of joint (with the TAIGA-HiSCORE array) events will increase by almost a factor of 10 and a high efficiency of the selection of events from gamma-ray photons will be retained for joint events. At present, the prototype of such a telescope, the Small Imaging Telescope (SIT) that uses silicon PMTs as imaging detectors, operates in the facility [29].

3. EAS PARAMETER RECONSTRUCTION METHODS

The EAS parameters reflecting the energy and mass A of the primary nucleus are measured to investigate the CR energy spectrum and mass composition by the EAS detection method. Since ~80% of the energy of the primary nucleus during the development of a cascade in the atmosphere passes into the electromagnetic component (electrons and photons), the total Cherenkov light flux from an EAS is a good measure of the primary energy, being independent of the mass number. However, it is impossible to measure the Cherenkov light flux at most arrays and, therefore, the flux density at a certain distance from the axis is chosen as a measure of the total flux. The depth of EAS maximum X_{max} is a parameter sensitive to the mass number. The depth of maximum for individual EASs fluctuates greatly ($\sigma(X_{max})$) for protons ~60–80 g cm^{-2}, depending on the energy; the mean value of X_{max} ($\langle X_{max} \rangle$) for the EAS from a nucleus with a mass number A is well described by a simple fit [30]:

$$\langle X_{max} \rangle = A + B \log E \text{ [TeV]}/A, \qquad (1)$$

with constants A and B (A = 370 g cm^{-2} and B = 65 g cm^{-2}).

In principle, the values of these parameters depend on the energy range under study, but, to a first approximation, this dependence may be neglected. As the energy changes by a factor of 10, $\langle X_{max} \rangle$ increases approximately by 65 g cm^{-2}. The change in $\langle X_{max} \rangle$ when passing from a proton to an iron nucleus is 110–120 g cm^{-2} in the range 10^{16}–10^{18} eV. The simulation results presented in Section 4 qualitatively coincide with this simple fit.

3.1. Reconstructing the Primary Particle Energy from Cherenkov Light

For arrays with a detector spacing ~100 m (Tunka-133 and TAIGA-HiSCORE) the primary particle energy is reconstructed from the Cherenkov light flux density at a distance of 200 m from the EAS axis (Q_{200}). The lateral distribution function (LDF) obtained from Monte Carlo simulations is used for the recalculation to a distance of 200 m. As simulations show [10] (Fig. 4), at such a distance from the axis the light flux density for a fixed energy depends weakly on the depth of EAS maximum X_{max} and EAS zenith angle.

The relation between the primary particle energy and Q_{200} derived from Monte Carlo simulations (CORSIKA, QGSJET-II-04) can be expressed by the following formula [13]:

$$E_0 = CQ_{200}^g, \qquad (2)$$

where $g = 0.94$ for the range 10^{16}–10^{17} eV and $g = 0.95$ for the range 10^{17}–10^{18} eV. The results of our computation are presented in Fig. 5.
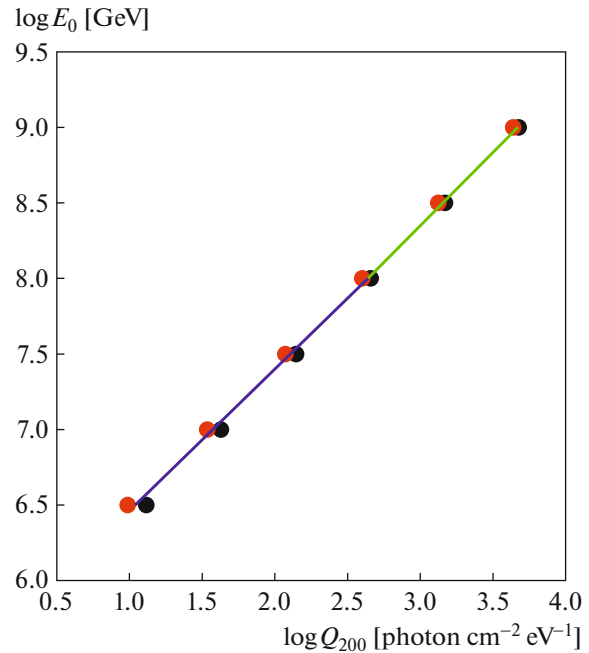
$\log Q$ [photon cm^{-2} eV^{-1}]
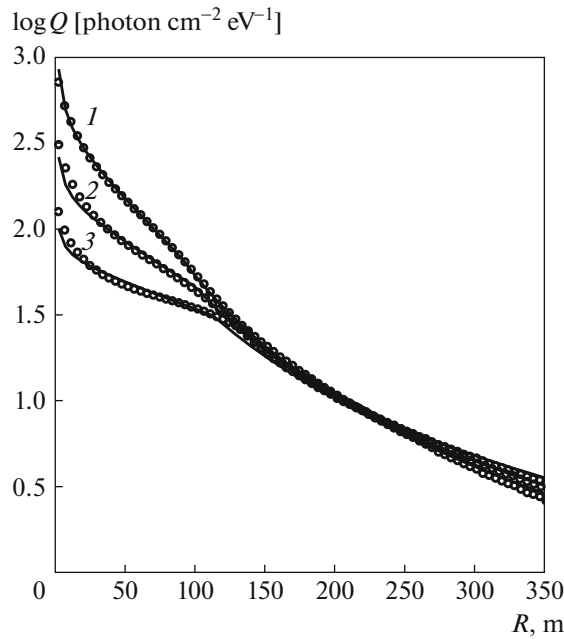
Fig. 4. The lateral distribution function of light from an EAS with an energy of 5×10^{15} eV computed with the CORSIKA code for various distances from the shower maximum to the array, $H_{max} = $ (*1*) 3.2, (*2*) 4.1, and (*3*) 5 km.

$\log E_0$ [GeV]

Fig. 5. Computation (CORSIKA, QGSJET-II-04) of the correlation between the primary particle energy (E_0) and the light flux density at a distance of 200 m from the axis (Q_{200}). The black dots indicate the mean values of Q_{200} for primary protons; the red dots indicate the mean values of Q_{200} for primary iron nuclei.

The constant C is determined by normalizing the derived experimental integral energy spectrum to the known total flux of CRs with an energy above 3×10^{15} eV measured in the QUEST experiment [31].

The relative error of the reconstructed shower parameters can be estimated by the well-known chessboard method [32]. For energies $E_0 \geq 10^{16}$ eV the EAS axis position reconstruction error is less than 6 m for the central part of the Tunka-133 array ($R \leq 450$ m) and less than 10 m for $450 \text{ m} \leq R \leq 800 \text{ m}$ and $E_0 \geq 5 \times 10^{16}$ eV. Given the uncertainty in the mass composition and the EAS axis position determination accuracy, the energy reconstruction error is ~10%. The presence of the Tunka-Rex array recording the EAS radio emission in the TAIGA astrophysical facility and of the LOPES array in the KASCADE-GRANDE array has allowed the EAS energy reconstruction accuracies between Tunka-133 and KASCADE-GRANDE to be compared [33]. The idea of the method is to compare the amplitudes of the signals from the Tunka-Rex and LOPES radio antennas, depending on the EAS energies reconstructed using the techniques developed in the Tunka-133 and KASCADE-GRANDE experiments. The systematic difference in measuring the energy turned out to be 5%.

The main EAS parameters for the TAIGA-HiSCORE array are reconstructed using the same algorithms as those for the Tunka-133 array. At the same time, for the TAIGA-HiSCORE array it is possible to reconstruct the EAS Cherenkov light flux density at a distance of 200 m from the axis by interpolating the amplitudes measured with its optical stations located at distances greater or smaller than 200 m for 100% of the events only at EAS energies above 10^{15} eV, whereas the energy threshold of the TAIGA-HiSCORE array, when its four or more optical stations are triggered, is ~80 TeV for EASs from charged CR particles. Therefore, a different EAS parameter reconstruction algorithm was developed for lower energies. The axis position is defined as the centroid of the pulse amplitudes at 4–5 stations. The light flux density near the axis is calculated as a mean for two stations closest to the axis. The computation with the CORSIKA code showed that because of large light flux fluctuations, the energy measurement error near the EAS axis is considerably larger than that from the light flux density at a distance of 200 m from the axis, but, on average, the light flux can be transformed to the EAS energy using the formula [34]

$$\log(E_0) = C + 0.87 Q_{65}, \qquad (3)$$

where Q_{65} is the photon flux density at a distance of 65 m from the axis.
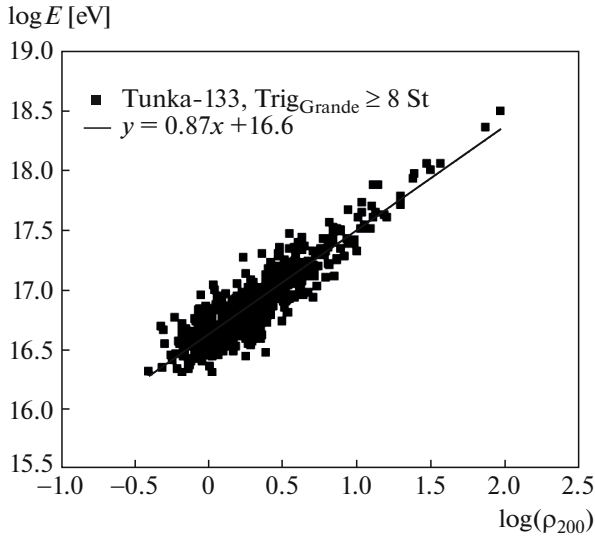
Fig. 6. Correlation between the EAS energy reconstructed from the Tunka-133 data and the charged particle density at a distance of 200 m from the axis from the Tunka-Grande data.

Fig. 7. Relationship between the LDF steepness $P = Q_{80}/Q_{200}$ and the thickness of the atmosphere between the array and the depth of EAS maximum ΔX_{max} [35] from the bank of events obtained by the Monte Carlo method.

3.2. Reconstructing the Primary Particle Energy from Charged EAS Particles

For the Tunka-Grande array the primary particle energy is reconstructed from the EAS particle flux density at a distance of 200 m from the axis [14]:

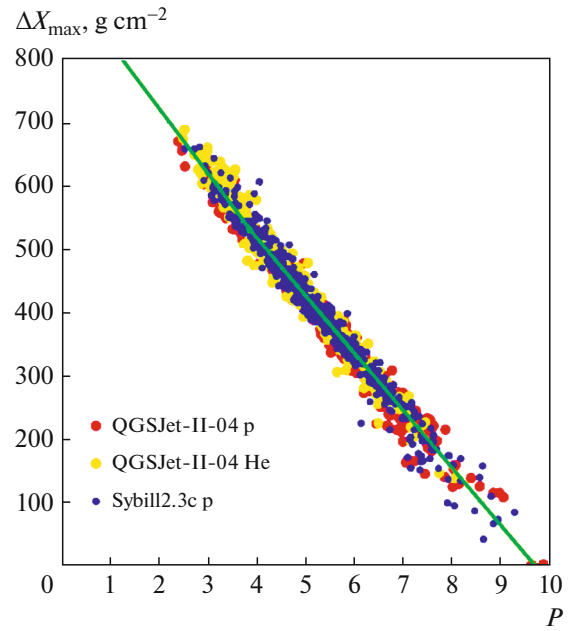$$\log(E/1 \text{ eV}) = C_a \log(\rho_{200}) + C_b. \tag{4}$$

The coefficients C_a and C_b in this expression are determined by substituting the EAS energy reconstructed from the Tunka-133 data into the left-hand side of the equation for the events recorded by both Tunka-Grande and Tunka-133. The experimental dependence of E on ρ_{200} is shown in Fig. 6.

3.3. Reconstructing the Depth of EAS Maximum

The parameter P that characterizes the steepness of the LDF of Cherenkov light is used to determine the depth of EAS maximum (X_{max}). P is defined as the ratio of the light flux at a distance of 80 m from the EAS axis, Q_{80}, to the flux at a distance of 200 m, Q_{200}:

$$P = Q_{80}/Q_{200}. \tag{5}$$

Our Monte Carlo simulations confirmed that the parameter P is determined only by the thickness of the atmosphere between the array and the depth of maximum ($\Delta X_{max} = 965/\cos\theta - X_{max}$ [g cm^{-2}]) and does not depend on the energy, shower zenith angle, and type of the primary nucleus (see Fig. 7). Here, 965 g cm^{-2} is the depth of the atmosphere at the loca-

tion of the arrays [35]. The calculated relation between ΔX_{max} and parameter P is nearly linear for the P range from 2.5 to 9. The standard deviation of the points from the fit for this range is ~15 g cm^{-2}. The computed points for heavier nuclei or zenith angles greater than 30° lie largely at values of the parameter P less than 2.5, i.e., refer to the events with LDPs that are virtually flat near the EAS axis for which the described method is inapplicable.

4. MAIN RESULTS

4.1. Energy Spectrum in the Range $10^{14}-10^{18}$ eV

The Tunka-133 and TAIGA-HiSCORE data obtained in 2175 and 327 h of operation, respectively, were used to construct the CR energy spectrum from the data of the TAIGA astrophysical facility. The joint CR energy spectrum [13, 34] is shown in Fig. 8 in comparison with the spectrum obtained previously from the Tunka-25 data [10]. The spectrum spans four orders of magnitude in the energy range from 3×10^{14} to 3×10^{18} eV. One of the main results that follows from the spectrum obtained is the proof of a more complex energy dependence of the CR intensity than was assumed previously. Apart from the "classical knee" at an energy of 3×10^{15} eV, two statistically significant features are observed in the spectrum. More specifically, at 2×10^{16} eV the slope of the energy spectrum decreases approximately by 0.2, while at 3×10^{17} eV the
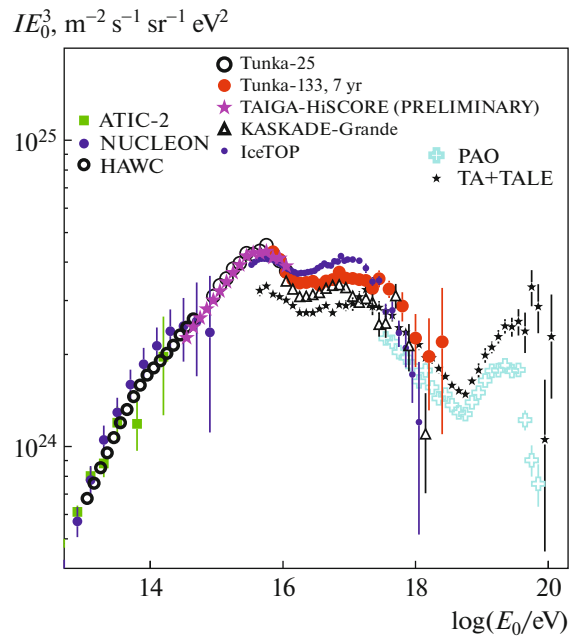
IE_0^3, m^{-2} s^{-1} sr^{-1} eV^2
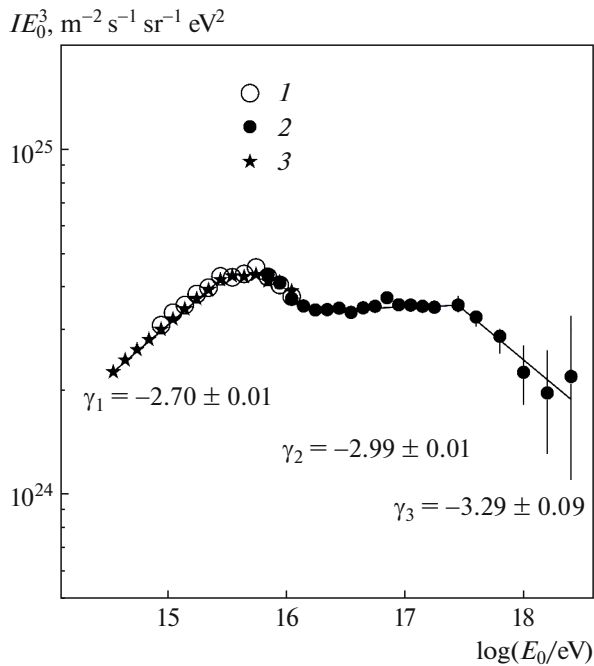
Fig. 8. CR energy spectrum based on data from the arrays of the TAIGA astrophysical facility: *1* — Tunka-25 [10], *2* — Tunka-133 [130, and *3* — TAIGA-HiSCORE [34].

IE_0^3, m^{-2} s^{-1} sr^{-1} eV^2

Fig. 9. Comparison of the CR energy spectra obtained in various experiments in a wide energy range: ATIC-2 [36], NUCLEON [37], HAWC [38], Tunka-25, TAIGA-HiSCORE, Runka-133, KASKADE-Grande [39], Ice-Top [40], PAO [41], and Ta+Tale [42].

slope of the spectrum again increases approximately by 0.3. The energy spectrum at energies below 3×10^{15} eV can be described by a power law with an index of 2.70 ± 0.01. In the energy range 2×10^{16}–3×10^{17} eV the spectrum is also described by a power law with an index of 2.99 ± 0.01. At energies above 3×10^{17} eV the slope of the spectrum increases to 3.29 ± 0.09. The steepening of the spectrum at 3×10^{17} eV can be interpreted as the "second knee" in the energy spectrum associated with the transition from galactic CRs to extragalactic ones. Figure 9 compares our data with the data of other experiments. There is good agreement both with the direct measurements at high-altitude balloons [36], satellite [37], and mountain [38] measurements at low energies and with the measurements at giant arrays at extremely high energies (the Pierre Auger Observatory (PAO) [41] and the TA array [42]). A decrease in the slope of the spectrum at 1.5–2.5×10^{16} eV by 0.2–0.3 is observed in all of the experimental data. At present, this effect has no astrophysical explanation.

4.2. Mass Composition in the Range 10^{15}–10^{18} eV

The mean depths of maximum derived at two arrays (Tunka-133 and TAIGA-HiSCORE) as a function of the primary particle energy are shown in Fig. 10. The data of both arrays, despite the difference in their geometry, agree well between themselves in the

wide energy range from 10^{15} to 3×10^{17} eV. Events with a zenith angle $\geq 30°$ and an energy at which the EAS detection efficiency is ~100% are chosen to obtain undistorted estimates of X_{max}. This energy is 1.25×10^{16} for Tunka-133 and 1.25×10^{15} eV for TAIGA-HiSCORE. In Fig. 10 our experimental data are compared with the X_{max} measurements obtained by the detection of fluorescent light from EASs at TA [42] and PAO [43] and a mixture of fluorescent and Cherenkov light in the TALE experiment [44]. All of the experimental results are compared with the theoretical curves computed with the QGSJET-II-04 model [45] for primary protons and iron nuclei. At a fixed energy X_{max} depends linearly on $\ln A$ (see Eq. (1)). Using this, the mean $\langle \ln A \rangle$ is usually determined by interpolation between the computed curves for protons and iron nuclei presented in Fig. 10. The result is shown in Fig. 11.

The energy dependence of the mean value of $\ln A$ is well extrapolated to the Auger results at 3×10^{17} eV [44] and contradicts the results of the much more complex (in interpreting the data) TALE experiment [43].
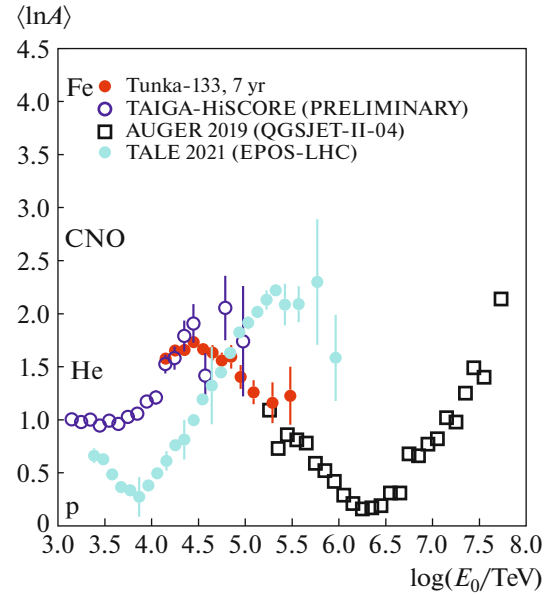
5. FACILITY DEVELOPMENT PLAN FOR THE NEAR FUTURE. CONCLUSIONS

The development of the astrophysical facility in the Tunka valley over 25 years has led to the construction of a number of serious arrays to study ultra-high-
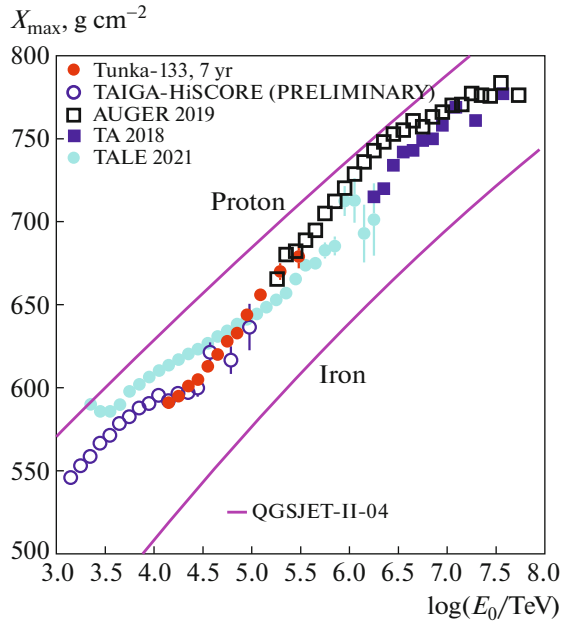
Fig. 10. Energy dependence of the mean X_{max}: Tunka-133 and TAIGA-HiSCORE [33], TA [42], TALE [43], and Auger [44].

Fig. 11. Energy dependence of the mean logarithm of the atomic number $\langle \ln A \rangle$: Tunka-133 and TAIGA-HiSCORE [33], TA [42], TALE [43], and Auger [44].

energy CRs. The energy spectrum pf primary CRs in a range of four orders of magnitude was reconstructed from the results obtained with these arrays. A number of features that haven not yet got an astrophysical interpretation are observed in the energy spectrum. First of all, the spectrum near the "first knee" at $(3-6) \times 10^{15}$ eV cannot be described simply as an abrupt change in the slope. At present, the feature in the spectrum at 2×10^{16} eV that was firmly established in a number of experiments has not been explained either. Finally, the energy at which the "second knee" is located is still determined with a great uncertainty. According to our data, light nuclei, protons and helium, must dominate in the CR flux in the range $10^{15}-10^{17}$ eV. This contradicts the break in the energy spectrum of the light CR component obtained at the ARGO-YBJ array at 0.7×10^{15} eV.

It should be noted that, according to the data on the mass composition in the region of the first knee obtained in various experiments, it is so far impossible to determine a consistent picture. It is possible that a detailed CR mass composition in this energy range will be ultimately understood only after the launch of a massive (several tons) detector [47] in a near-Earth orbit. In the coming 2−3 years the study of the mass composition will be continued at the astrophysical facility as one of the main themes. An attempt will be made to study the mass composition at energies below 10^{15} eV, possibly, based on the joint TAIGA-HiSCORE and TAIGA-IACT data. In the range $10^{16}-10^{18}$ eV we hope to advance in studying

the mass composition through an increase in the area of the muon detectors. We also associate the progress at energies above 10^{17} eV with the possible deployment of a new fluorescent detector in the TAIGA astrophysical facility.

REFERENCES

1. N. M. Budnev, I. I. Astapov, P. A. Bezyazeekov, et al., Nucl. Instrum. Methods Phys. Res., Sect. A **958**, 162113 (2020).

2. L. A. Kuzmichev, I. I. Astapov, P. A. Bezyazeekov, et al., Phys. At. Nucl. **81**, 497 (2018).

3. M. G. Aartsen, M. Ackermann, J. Adams, et al., Science (Washington, DC, U. S.) **361**, 6398 (2018); arXiv: 1807.08816.

4. A. D. Avrorin, A. V. Avrorin, V. M. Aynutdinov, R. Bannash, I. A. Belolaptikov, V. Brudanin, N. M. Budnev, A. A. Doroshenko, G. V. Domogatsky, R. Dvornický, A. N. Dyachok, Zh.-A. M. Dzhilkibaev, L. Fajtce, S. V. Fialkovsky, A. R. Gafarov, et al., JETP Lett. **108**, 787 (2018); arXiv: 1810.10966.

5. A. R. Bell, Astropart. Phys. **43**, 56 (2013).

6. P. Blasi, C. R. Phys. **15**, 329 (2014); arXiv: 1403.2967.

7. V. Ptuskin, EPJ Web Conf. **145**, 03001 (2017).

8. S. V. Bryanski, G. N. Dudkin, O. A. Gress, et al., in *Proceedings of the 24th International Cosmic Ray Conference ICRC, Roma* (1995), Vol. 2, p. 724.

9. R. Bagduev, V. Balkanov, I. Belolaptikov, et al., Nucl. Instrum. Methods Phys. Res., Sect. A **420**, 138 (1999).

10. N. Budnev, D. Chernov, O. Gress, et al., Astropart. Phys. **50−52**, 18 (2013).

11. O. Gress, I. Astapov, N. Budnev, et al., Nucl. Instrum. Methods Phys. Res., Sect. A **845**, 367 (2017).

12. S. Berezhnev, S. Epimakhov, N. Karpov, et al., Nucl. Instrum. Methods Phys. Res., Sect. A **692**, 98 (2012).

13. N. Budnev, A. Chiavassa, O. Gress, et al., Astropart. Phys. **117**, 102406 (2020).

14. R. Monkhoev, N. Budnev, A. Gafarov, D. M. Voronin, A. R. Gafarov, O. A. Gress, T. I. Gress, A. N. Dyachok, A. V. Zagorodnikov, V. L. Zurbanov, N. N. Kalmykov, Yu. A. Kazarina, S. N. Kiryuhin, E. E. Korosteleva, V. A. Kozhin, L. A. Kuzmichev, et al., Bull. Russ. Acad. Sci.: Phys. **83**, 959 (2019).

15. M. Tluczykont, D. Hampf, D. Horns, et al., Astropart. Phys. **56**, 42 (2014).

16. I. Astapov, N. Barbashina, A. Bogdanov, V. Boreyko, N. M. Budnev, R. Wischnewski, A. R. Gafarov, V. Grebenyuk, O. A. Gress, T. I. Gress, A. A. Grinyuk, O. G. Grishin, N. Gorbunov, A. N. Dyachok, S. N. Epimakhov, et al., Bull. Russ. Acad. Sci.: Phys. **81**, 460 (2017).

17. L. Kuzmichev, I. Astapov, P. Bezyazeekov, et al., EPJ Web Conf. **145**, 01001 (2017).

18. M. Tluczykont, N. Budnev, I. Astapov, et al., EPJ Web Conf. **136**, 03008 (2017).

19. A. D. Panov, I. I. Astapov, A. K. Awad, et al., arXiv: 2109.09637.

20. P. Bezyazeekov, N. Budnev, O. Gress, et al., Nucl. Instrum. Methods Phys. Res., Sect. A **802**, 89 (2015).

21. D. Kostunin, P. Bezyazeekov, N. Budnev, et al., PoS (ICRC2019) 319 (2019); arXiv: 1908.1035.

22. A. Ivanova, N. Budnev, A. Chiavassa, et al., J. Instrum. **15**, C06057 (2020).

23. I. Astapov, P. Bezyazeekov, A. Borodin, et al., Nucl. Instrum. Methods Phys. Res., Sect. A **936**, 254 (2019).

24. L. Kuzmichev, I. Astapov, P. Bezyazeekov, et al., Nucl. Instrum. Methods Phys. Res., Sect. A **952**, 161830 (2020).

25. N. Budnev, I. Astapov, P. Bezyazeekov, et al., J. Instrum. **15**, C09031 (2020).

26. B. Acharya, M. Actis, T. Aghajani, et al., Astropart. Phys. **43**, 3 (2013).

27. A. Grinyuk, E. Postnikov, P. Volchugov, et al., PoS (ICRC2021) **395**, 713 (2021).

28. E. Postnikov, A. Grinyuk, L. Kuzmichev, et al., EPJ Web Conf. **145**, 19005 (2017).

29. D. Chernov, I. Astapov, P. Bezyazeekov, et al., J. Instrum. **15**, C09062 (2020).

30. K.-H. Kampert and M. Unger, Astropart. Phys. **35**, 660 (2012).

31. E. Korosteleva, V. Prosin, L. Kuzmichev, et al., Nucl. Phys. B Proc. Suppl. **165**, 74 (2007).

32. A. Karle, M. Merck, R. Plaga, et al., Astropart. Phys. **3**, 321 (1995).

33. W. Apel, J. Arteaga-Velázquez, L. Bahren, et al., Phys. Lett. B **763**, 179 (2016).

34. V. Prosin, I. Astapov, P. Bezyazeekov, et al., Bull. Russ. Acad. Sci.: Phys. **83**, 1016 (2019).

35. V. Prosin, I. Astapov, P. Bezyazeekov, et al., Bull. Russ. Acad. Sci.: Phys. **85**, 395 (2021).

36. A. Panov, J. Adams, Jr., H. Ahn, G. L. Bashinzhagyan, J. W. Watts, J. P. Wefel, J. Wu, O. Ganel, T. G. Guzik, V. I. Zatsepin, I. Isbert, K. C. Kim, M. Christl, E. N. Kouznetsov, M. I. Panasyuk, et al., Bull. Russ. Acad. Sci.: Phys. **73**, 564 (2009).

37. A. Turundaevskiy, O. Vasiliev, D. Karmanov, I. M. Kovalev, and I. A. Kudryashov, Bull. Russ. Acad. Sci.: Phys. **85**, 353 (2021).

38. R. Alfaro, C. Alvarez, R. Arceo, et al., Phys. Rev. D **96**, 122001 (2017).

39. W. Apel, J. Arteaga Velázquez, K. Bekk, et al., Astropart. Phys. **36**, 183 (2012).

40. M. G. Aartsen, R. Abbasi, Y. Abdou, et al., Phys. Rev. D **88**, 042004 (2013).

41. J. Abraham, P. Abreu, M. Aglietta, et al., Phys. Lett. B **685**, 239 (2010).

42. R. Abbasi, M. Abe, T. Abu-Zayyad, et al., Astrophys. J. **858**, 76 (2018).

43. A. Yushkov, A. Aab, P. Abreu, et al., PoS (ICRC2019), 482 (2019); arXiv: 1909.09073.

44. R. Abbasi, M. Abe, T. Abu-Zayyad, et al., Astrophys. J. **909**, 178 (2021).

45. S. Ostapchenko and M. Bleicher, Phys. Rev. D **93**, 051501 (2016).

46. B. Bartoli, P. Bernardini, X. J. Bi, et al., Phys. Rev. D **92**, 092005 (2015).

47. D. Podorozhny, D. Karmanov, A. Panov, et al., Bull. Russ. Acad. Sci.: Phys. **83**, 637 (2019).

Translated by V. Astakhov